基于神经网络优化的车身镀锌板点焊性能预测

赵 欣， 张延松， 陈关龙， 张小云
（上海交通大学 机械与动力工程学院，上海 200240）

摘 要：针对汽车车身常用的镀锌钢板（GMW2 和 DP600）的点焊性能预测问题进行了研究，引入人工神经网络模型来描述点焊工艺参数空间同焊点接头质量空间的映射关系；在对普通网络存在的缺陷问题进行深入分析的基础上，结合大量试验综合考虑，对网络模型进行了优化改进；然后将试验得到的大量点焊工艺参数与相应点焊接头质量的试验数据提供给神经网络学习。结果表明，学习后的优化神经网络模型能够准确有效地预测焊接电流对点焊熔核直径、压痕深度以及拉剪强度的影响规律。亦即该优化神经网络模型可有效地实现对车身镀锌钢板点焊性能的预测，且预测精度和准确率较高，符合工程需要，具有一定的实用价值。

关键词：车身镀锌钢板；点焊；人工神经网络；预测；优化
中图分类号：TG453.9 文献标识码：A 文章编号：0253－360X(2006)12－077－05

赵 欣

0 序 言

作为现代汽车车身制造中应用最广泛的装配工艺方式，电阻点焊占据了整个车身装配工作量的90%以上。如一辆轿车白车身约由3 000～6 000个焊点将数百个薄板冲压零件拼装而成。因此，对电阻点焊质量进行良好的监测和控制是十分必要的。由于电阻点焊过程是一个热、电、磁多场耦合的复杂过程，各工艺参数间关系复杂，干扰因素多，尤其是焊接过程的短时性和形核过程的不可见性，使得对其建立精确的数学模型非常困难。目前工程上采用的恒流控制法、电极位移检测法等动态质量监控方法均无法达到非常满意的效果[1]。

人工神经网络ANN（artificial neural network）在焊接中的应用始于20世纪90年代，起初主要应用于弧焊，现已推广到点焊，在焊接过程控制、焊接缺陷检测以及接头性能预测等方面均有应用[2～4]。利用ANN很强的非线性映射能力和适用于多信号融合的特点，在无假设情况下，通过网络训练，学习大量的试验数据，利用其非线性映射的泛化能力自动抽取所学习数据的关键特征，来描述点焊的工艺参数空间与焊点接头质量空间的映射关系，从而实现对焊点接头质量的预测[3]。目前国内外相关研究主要针对不同材料或各种焊接类型进行建模仿真，在模型优化及预测效果上的研究尚待进一步深入[4]。

文中针对在现代车身制造中使用比重日益增大的镀锌钢板进行研究。由于锌层的影响，其点焊性能较之普通低碳钢板差异较大。在国内外现有相关研究的基础上，将试验所得的大量的车身镀锌钢板点焊工艺参数与相应焊点接头质量的试验数据提供给ANN进行学习，并结合学习情况对所建立的模型进行优化，从而改善其预测精度及准确率。通过大量的试验和仿真，优化后ANN模型可实现较为理想的预测精度及准确率。

1 试验系统简介

文中所用的试验材料是北美通用汽车公司（GM）采用的两种标准热镀锌钢板，分别为GMW2（低碳钢）和DP600（高强度钢）两种规格，抗拉强度分别为350 MPa和600 MPa，单位面积锌层质量 $\rho=60\ g/m^2$。通过改变焊接电极力、焊接电流和焊接时间，进行大量的点焊试验，确定了这两种材料的点焊工艺参数作为文中试验系统的基础，如板厚为0.8 mm的材料的点焊工艺参数为：保持焊接时间为10个周波（0.2 s），电极力为2.2 kN，焊接电流在7～12 kA范围内变化。

焊接设备为集成在机器人上的SRTC型伺服焊机。相对于传统的气动焊机，该伺服焊机能实现对

收稿日期：2005－12－05
基金项目：国家自然科学基金资助项目（50575140）；高校博士点基金资助项目（20050248028）

电极速度、位置、力、电流和时间的精确控制[5]，有利于产生更精确的焊接工艺参数输入样本，保证对ANN模型更有效的训练。此外，利用焊机伺服编码器反馈的电极位移还可在线获得焊点压痕值。相关研究表明，压痕也能表征点焊接头质量信息[6]。

试验方法为在有效的工艺参数下，通过金相试验测量焊点熔核直径 d；通过万能材料试验机测量焊点拉剪强度 σ_τ；通过伺服焊机获得焊点压痕深度 s。取 d，s 以及拉剪强度比 n 为点焊接头的质量评价参数(其中 $n=\sigma_\tau/R_m$，R_m 为母材抗拉强度)。试验中所用的试样尺寸为：100 mm×25 mm×0.8 mm。

2 系统建模及优化

2.1 网络模型的建立

研究中首先采用的是误差反向传播算法(back propagation network)，简称 BP 神经网络，由于其具有算法简单、易实现、计算量较小、并行性强等优点，目前仍是多层前向神经网络训练的首选算法[7]。建模时主要考虑了 BP 网络隐含层数的选择和隐含层单元数的选择。在训练过程中发现，一个 3 层 BP 网络即可完成任意 n 维空间到 m 维空间的映射；且采用 2 个隐含层并不会比采用 1 个隐含层更容易减小最后的训练误差，却要花费长得多的训练时间，因此，选用 3 层 BP 网络，以电阻点焊每个周波的电流有效值和电极间电压为网络输入，以熔核直径、压痕深度和拉剪强度比为网络输出。即输入层节点数为 20 个，输出层节点为 3 个，结合经验公式(1)并经试验确定，当取 $a=5$，$n_1=10$ 时，系统具有相对较好的识别效果。网络结构为 20—10—3，如图 1 所示。

$$n_1=\sqrt{n+m}+a, \tag{1}$$

式中：n、m 和 n_1 分别为输入、输出和隐含层节点数；a 为 1～10 之间的常数，经试验确定。

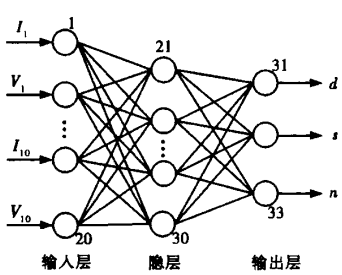

图 1 系统 BP 网络结构图

Fig. 1 Structure of system BP networks

2.2 网络模型的优化

传统的 BP 算法由于算法本身的不完备性，存在易陷入局部最小点；“伪饱和”现象会导致网络瘫痪；收敛速度慢和训练时间太长等缺陷[8～10]。在模型仿真过程中，针对这些缺陷问题进行了反复试验和对比分析，综合各种改进方案，对初始的 BP 模型进行优化，以提高网络的训练效率。

(1) 严密监控网络训练过程，发现网络陷入局部最小点时，及时修改权值矩阵 W 和 V 的初值并重新训练，使网络“逃离”局部最小点[8]。式(2)为误差测度函数，可见网络的误差曲面是一高维空间中的复杂不规则曲面，其中分布着许多局部最小点。

$$E=\frac{1}{2}\sum_{k=1}^{m}(y_k-o_k)^2, \tag{2}$$

式中：y_k 和 o_k 分别为期望输出和实际输出。采用在网络激活函数(sigmoid 函数)中加入 μ 因子等方法，如式(3)，也有助于误差离开平坦区域或局部最小点，平稳收敛，但收敛速度也会随之下降，因此在离开平坦区后应使 μ 恢复或在节点误差调整中另加入比例因子 σ，使收敛速度提高[8]。

$$f(\mathrm{net})=(1+\mathrm{e}^{-\mathrm{net}/\mu})^{-1}, \tag{3}$$

式中：net=XW 为神经元的网络输入累积效果。

(2)采用变学习率[9]或变步长等方法，可有效地避免“伪饱和”现象。权值累积到一定程度会使网络输入变得很大，且使其激活函数的导函数在此点取值很小，从而极大地降低了训练步长，最终导致网络停止收敛。要防止该现象的发生，要注意在初始化网络联接权矩阵时，采用不同的小伪随机数。

(3)提高网络收敛速度、缩短训练时间的手段很多，如在权值调整中加入动量因子 mc；通过试验确定 μ 因子和比例因子 σ 的适当组合；不同层采用不同学习率[9]等，均能有效地加速收敛并防止振荡。

结合以上分析，对含动量项的变学习率算法、弹性 BP 算法、变尺度共轭梯度法、一阶正割准牛顿算法以及 Levenberg-Marquardt 算法这五种改进 BP 算法进行综合优化[10]，综合考虑它们在训练收敛速度、学习稳定性、存储量和计算量等方面上各自的优势，以确定的网络训练样本、网络参数和综合改进的优化 BP 算法对 20—10—3 的初始 BP 网络进行 10 000 次训练，得到如图 2 所示的训练过程结果：其中动态均方根误差(root-mean-square error, RMSE)为 0.010 52；对比初始 BP 模型，在相同样本条件下训练 10 000 次，结果如图 3 所示，其中 RMSE=0.019 69。由此可见，经综合优化改进后的 BP 模型在训练效率(收敛速度)、学习稳定性以及存储量和计算量等各方面上均优于原算法。

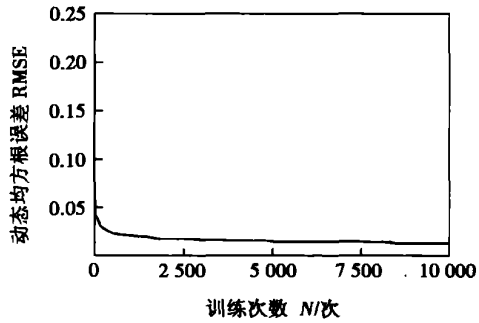

图 2　综合改进 BP 优化模型的网络训练

Fig. 2　Network training process of synthetically optimized BP model

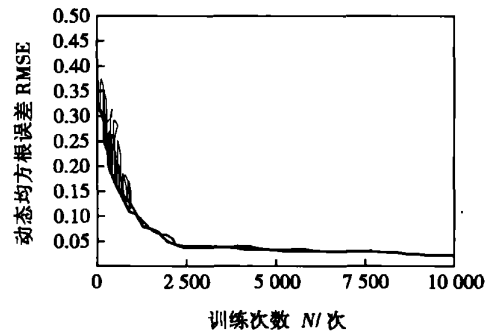

图 3　初始 BP 模型的网络训练

Fig. 3　Network training process of original BP model

3　点焊性能预测及分析

研究中首先对 A(GMW2)和 B(DP600)两种热镀锌钢板材料的试样，在一定的通电时间 t_w 和电极力 F_w 下，通过改变焊接电流的大小，测得各试样在不同焊接条件下焊点的熔核直径 d、压痕深度 s 及拉剪强度比 n；然后对所得试验数据进行分析筛选，剔除严重畸变数据，最后确定神经网络的训练样本 77 个，检验样本 16 个。将由试验数据处理后得到的 A 和 B 的训练样本分别输入给神经网络进行学习，学习后的网络可完成对相应焊接条件下的焊点熔核直径、压痕深度以及拉剪强度的预测。如图 4，5，6 所示分别为焊接电流同熔核直径、压痕深度及拉剪强度比的关系预测曲线。由图中可以看出：(1) 焊接电流同熔核直径关系(I-d)，焊接电流同压痕深度关系(I-s)，焊接电流同拉剪强度比关系(I-n)预测曲线均大致呈递增趋势，符合实际情况：即在一定范围内随着焊接电流的增加，焊点熔核直径及拉剪强度也增大，压痕变深。(2) 电流较小(< 8 kA)时，各试验值均很小；电流较大(> 11 kA)时，d，s 的试验值很

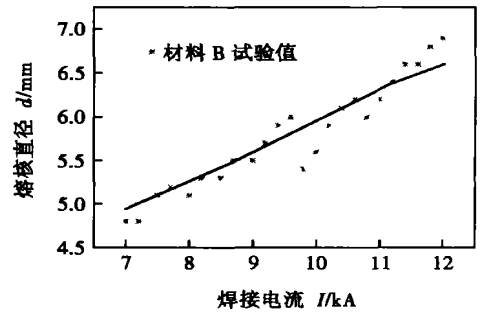

图 4　焊接电流与熔核直径关系的 ANN 预测曲线

Fig. 4　Relationship between welding currents and nugget diameters predicted by ANN

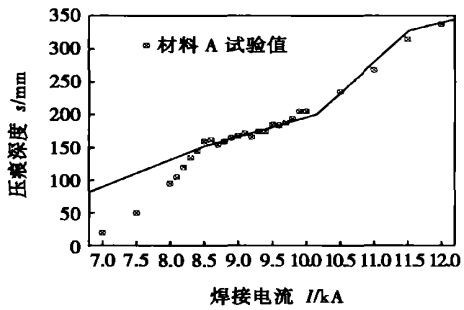

图 5　焊接电流与压痕深度关系的 ANN 预测曲线

Fig. 5　Relationship between welding currents and indentation depth predicted by ANN

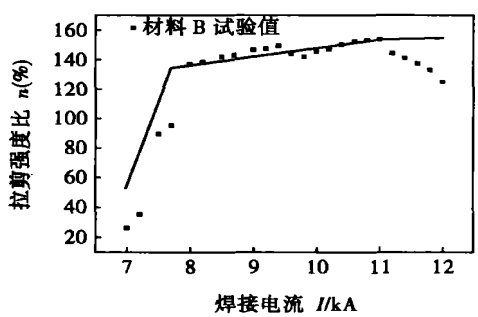

图 6　焊接电流与拉剪强度比关系的 ANN 预测曲线

Fig. 6　Relationship between welding currents and tensile-shear strength predicted by ANN

大但 n 的试验值反而降低。这同对应的预测值并不一致，从而反映了该模型预测是在一定输入值范围内有效的。(3) 该两种材料的锌层厚度较厚，受其影响，试验中随焊接电流的增大，较易出现喷溅甚至电极粘连，加速材料焊接性能的恶化。这也是解释图中某些试验值同预测值的偏差较大的重要原因。(4) 由图 5 可知，点焊 0.8 mm 厚 GMW2 镀锌钢板的有效电流范围应为 8.5 ~ 10 kA，否则压痕深度

将过浅或过深，焊点质量差；由图 6 可知，点焊 0.8 mm 厚 DP600 镀锌钢板的有效电流范围应为 8～11 kA，否则所形成的熔核强度将明显不够。这些同实际情况均是相符的。

综上所述，经训练后的优化神经网络模型能较为准确地预测焊接电流对镀锌钢板点焊性能的影响规律，并能正确地反映出点焊的基本原理。

4 预测精度分析

用16个检验样本对训练后的优化神经网络模型进行检验。如表 1 所示，结果表明，焊点熔核直径的有效平均预测误差不超过 4%，最大相对误差为 9.87%；压痕深度的有效平均预测误差不超过 4%，最大相对误差为 10.00%；拉剪强度的有效平均预测误差不超过 8%，最大误差为 12.34%。预测相对误差较大的个别样本是由于样本本身的输入误差和噪声导致样本失真而引起的，如表 1 中的样本 2，3，9，13（其中，样本 9 即是由于输入焊接电流样本失真从而导致预测失准的）。而同时，整个网络模型的输出并未因这些干扰和误差而造成误输出，这恰好反映了该优化人工神经网络具有很强的容错性和聚类性。

表 1 DP600 和 GMW2 镀锌钢板样本预测结果

Table 1 Sample verifying results of DP600 and GMW2 galvanized steel sheets

编号	输入参数均值		输出参数实测值			输出参数预测值			相对误差		
	焊接电流 I/kA	极间电压 U/V	熔核直径 d/mm	压痕深度 s/μm	拉剪强度 σ_τ/MPa	熔核直径 d'/mm	压痕深度 s'/μm	拉剪强度 σ_τ'/MPa	熔核直径 (%)	压痕深度 (%)	拉剪强度 (%)
1	8.022	0.854	5.1	95	338.2	5.178	98	345.05	1.53	3.16	2.03
2	8.196	0.855	5.3	120	369.5	5.823	108	415.08	9.87	10.00	12.34
3	8.428	0.868	5.3	151	390.3	5.412	138	410.02	2.11	8.61	5.05
4	8.629	0.863	5.5	160	403.4	5.602	165	420.86	1.85	3.13	4.33
5	8.827	0.868	5.6	163	421.1	5.711	165	445.05	1.98	1.23	5.64
6	9.018	0.873	5.9	170	404.4	6.119	173	427.04	3.71	1.76	5.57
7	9.217	0.882	5.9	168	421.0	6.097	172	450.76	3.34	2.38	7.07
8	9.454	0.891	6.1	180	442.5	6.025	175	462.08	1.23	2.78	4.41
9	9.057	0.897	5.7	172	840.7	5.298	165	860.77	7.05	4.07	2.39
10	9.461	0.909	5.9	185	853.9	5.991	188	897.19	1.54	1.62	5.05
11	9.625	0.917	6.1	188	862.7	5.921	185	902.42	2.93	1.60	4.63
12	9.809	0.939	5.5	201	871.5	5.652	206	918.53	2.76	2.49	5.41
13	10.021	0.956	5.7	210	881.9	6.024	225	921.05	5.68	7.14	4.42
14	10.198	0.966	5.9	222	891.2	6.112	230	935.15	3.59	3.60	4.91
15	10.621	0.978	6.3	254	892.9	6.425	263	948.88	1.98	3.54	6.28
16	11.093	0.989	6.6	277	891.1	6.438	288	957.55	2.45	3.97	7.42

5 结 论

（1）普通 BP 神经网络模型在经过综合优化改进后，网络的稳定性和收敛速度均大为改善，网络训练时间得到有效地缩短，这将为 ANN 在焊接工业上更广更深的应用提供有益的借鉴。

（2）优化后的神经网络模型接受样本训练之后，能够较为准确地预测一定范围内的焊接电流对车身热镀锌钢板点焊性能的影响规律，并正确地反映出点焊的基本原理。

（3）所建网络模型的预测精度和准确率能满足工程上的需要，可作为实现电阻点焊质量的精确在线监控以及无损检测的重要基础。

参考文献：

[1] Jou Min. Real time monitoring weld quality of resistance spot welding for the fabrication of sheet metal assemblies[J]. Journal of Materials Processing Technology, 2003, 132(10): 1－3.

[下转第 84 页]

3 结 论

(1) 焊缝的表面不平度会直接影响超声信号的传播,对缺陷的检测造成影响。当表面不平度过大时,会给纵波入射检测造成很大困难。焊缝表面不平度较小时,可以通过选取适当的探头对焊缝进行纵波检测。

(2) 高频窄脉冲聚焦探头适于检测近表面的小缺陷,其检测灵敏度高,在现有检测条件下,可以发现焊缝表面不平度较小的试件表面以下 1.0~2.5 mm 深的范围内、直径 0.3 mm 以上的缺陷。

参考文献:

[1] 周振丰, 张文钺. 焊接冶金与金属焊接性[M]. 北京: 机械工业出版社, 1987.

[2] 郭 鹏, 杨家林. TC4 钛合金精密焊接工艺研究[J]. 机械, 2001, 28(4): 35—36.

[3] 张 旭. 钛合金材料焊接工艺和质量控制的探讨[J]. 化工设备与管道, 2002, 39(4): 59—62.

[4] Greenwood M S, Minachi A, Thompson R. Effects of surface conditions on an ultrasonic inservice inspection[J]. Materials Evaluation, 2000, 32(5): 439—448.

[5] 陈文革, 魏劲松. 超声无损检测的应用研究与进展[J]. 无损探伤, 2001, 25(4): 1—3.

[6] 张小飞, 王 茁, 周有鹏. 超声检测中的噪声处理[J]. 无损检测, 2002, 24(5): 200—202.

作者简介: 郭立伟, 女, 1971 年出生, 博士研究生。主要从事无损检测方面的科研和教学工作, 发表论文 10 余篇。

Email: guoliwei2816@sohu.com

[上接第 80 页]

[2] Ivezic N, Alien J D, Zacharia T. Neural network-based resistance spot welding control and quality prediction[J]. Intelligent Processing and Manufacturing of Materials, 1999, 2(7): 10—15.

[3] 张忠典, 李 严. 人工神经元网络法估测点焊接头力学性能[J]. 焊接学报, 1997, 18(1): 1—4.

[4] Yongjoon Cho, Rhee S. Quality estimation of resistance spot welding by using pattern recognition with neural networks [J]. IEEE Transactions on Instrumentation and Measurement, 2004, 53(4): 330—334.

[5] 张延松, 许 敏, 陈关龙, 等. 伺服焊枪在轿车车身制造中的应用前景研究[J]. 汽车工程, 2004, 26(4): 504—507.

[6] Slavick, Stephen A. Using servoguns for automated resistance welding [J]. Welding Journal, 1999, 78(7): 29—33.

[7] Osman K A. Monitoring of resistance spot-welding using multi-layer perceptrons[J]. Artificial Neural Networks in Engineering, 1994, 4(1): 1109—1114.

[8] Jacques De Villiers. Back-propagation neural networks with one and two hidden layers [J]. IEEE Transactions on Neural Networks, 1992, 4(1): 136—144.

[9] 张忠典, 李学军, 杜 涛, 等. 用 BP 算法建立 ANN 模型时学习率的选取[J]. 焊接, 2004(1): 14—17.

[10] 金丕彦. BP 算法各种改进算法的研究及应用[J]. 南京航空航天大学学报, 1994, 11(1): 201—205.

作者简介: 赵 欣, 男, 1980 年 12 月出生, 博士研究生。主要研究车身连接工艺(点焊, 胶粘等)质量控制及在线检测, 发表论文 4 篇。

Email: zhxin@sjtu.edu.cn

spot surface.

Key words: resistance spot welding; image of welding spot surface; image processing; Radical Basic Function neural network; quality monitoring

Interface microstructure and mechanical property of CMT welding-brazed joint between aluminum and galvanized steel sheet SHI Chang-liang, HE Peng, FENG Ji-cai, ZHANG Hong-tao (State Key Laboratory of Advanced Welding Production Technology, Harbin Institute of Technology, Harbin 150001, China). p61—64

Abstract: Welding-brazing experiment of aluminum and galvanized steel was conducted with cold metal transfer method. The interface microstructure and mechanical property of the joint were analyzed by SEM, EDAX and transverse tensile test. The results indicate that good lap joint between aluminum and galvanized steel sheet can be made in appropriate parameters. The interface turns to be thin from middle to the edge with the components changing from $FeAl_3$ intermetallics to a compound of α solid solution and $FeAl_3$ intermetallics. Meanwhile, a rich-zinc zone composed of α solid solution and aluminum at the edge of weld metal exists. In the tensile test, fracture appears in the heat affected zone of aluminum base metal, and its tensile-strength is 72.09 MPa.

Key words: welding-brazing; cold metal transfer; intermetallics; interface; rich-zinc zone

Numerical calculations of residual stress in Ti(C, N)/40Cr brazed joint WU Ming-fang, ZHOU Xiao-li, MA Cheng, YANG Pei (Provincial Key Lab of Advanced Welding Technology, Jiangsu University of Science and Technology, Zhenjiang 212003, Jiangsu, China). p65—68

Abstract: To obtain the effect of copper and molybdenum interlayer on the residual stress of Ti(C, N)/40Cr brazed joint, the finite element mothod was conducted. The simulation results showed that the high tensile stress concentration with a maximum stress magnitude of 268 MPa happens at the narrow zone near ceramic/steel seam in the ceramic side without interlayer, but when the metal with copper foil of low yield stress was used as interlayer, the residual stress can be significantly decreased, and the maximum residual tensile stress reduce to 98 MPa, and there are to change of maximum genetic zone in brazed joint with interlyer and with out interlayer. When the low linear expansion coefficient metal molybdenum was used, the maximum stress occurred at the molybdenum interlayer zone, which gave a less residual stress reduction effect than copper foil. It also can be seen that the optimum interlayer thickness is about 0.8 mm for either interlayer kinds, and the thickness with thicker or thinner than 0.8 mm will be harmful to stress reduction efect.

Key words: Ti(C, N) based metal ceramic; 40Cr steel; brazing; residual stress; numerical calculation

Effects of shielding gas on microstructure and number of gas pore in high strength aluminum alloys weld XU Liang-hong, TIAN Zhi-ling, ZHANG Xiao-mu, PENG Yun (State Key Laboratory of Advanced Steel Processes and Products, Central Iron & Steel Research Institute, Beijing 100081, China). p69—73

Abstract: The effect of Ar and He dual mixed shielding gas and Ar, He and CO_2 ternary mixed shielding gas on the number of the gas pore and microstructure in the weld was studied in arc welding of 2519 aluminum alloy. Results indicate that, compared with using Ar alone, the number and the size of gas pore is reduced by using Ar and He dual mixed shielding gas and the dual mixed shielding gas is also helpful for the transition of columnar crystal to equiaxed crystal. When the percentage of He reaches 70%, the number and the size of the gas pore are reduced significatly, and in weld centre it can get the smallest equiaxed crystal entirely. When filling 1% CO_2 into the dual mixed gas which the ratio of Ar: He is 30∶69, the number of the gas pore is further reduced, but there is no evidence to prove that it can affect the microstructure of the weld. The width and the softening extent of the HAZ can also be reduced by filling He into Ar shielding gas.

Key words: high strength aluminum alloy; mixed shielding gas; gas pore; microstructure

Influence of hydrogen on weld metal toughness by self-shielded flux-cored wire welding SUI Yong-li[1,2], DU Ze-yu[1], HUANG Fu-xiang[1,2], TIAN Liang[3] (1. School of Materials Science and Engineering, Tianjin University, Tianjin 300072, China; 2. Pipeline Research Institute of CNPC, Langfang 065001, Hebei, China; 3. BeiJing University of Science & Technology, Beijing 100083, China). p74—76

Abstract: The effect of hydrogen content on the low temperature toughness of weld metal was studied by Nick-Break test, low temperature impact test and scanning electron microscopy test, which filled by self-shielded flux-cored welding wire and held different periods in room temperature. The results show that all these conditions such as the high content of hydrogen in self-shielded flux-cored wire, uneasy outflow of hydrogen from the weld metal and the short-lived molten pool, make the content of hydrogen high in weld metal (immediately test after welding). The average value of impact absorbing energy at low temperature is low and the data are disperse under the action of hydrogen and non-metallic inclusion. When the work piece stored 40 days in room temperature, the content of hydrogen decreases, and the fish eye decrease or disapear, and the average value of impact absorbing energy at low temperature increase and dispersion of the data decrease.

Key words: self-shielded flux-cored wire; pipeline; fish eye; impact absorbing energy

Performance prediction in spot welding of body galvanized steel sheets based on artificial neural network and its optimization ZHAO Xin, ZHANG Yan-song, CHEN Guan-long, ZHANG Xiao-yun (School of Mechanical Engineering, Shanghai Jiaotong University, Shanghai 200240, China). p77—80, 84

Abstract: The performance prediction in spot welding of the galvanized steel sheets are very important in the automobile body manufacturing. So it was studied with galvanized steel sheet GMW2

and DP600. Artificial neural networks (ANN) are used to describe the mapping relationship between welding parameters and welding quality. After analyzing the limitation of standard BP networks, the original model was optimized based on lots of experiments. Then a lot of experimental data about welding parameters and corresponding spot welding quality were supplied to the ANN for training. The results indicate that the improved BP network model can accurately predict the influence of welding currents on welding nugget diameters, depth of indentation and the tension-shear strength of welding spots. That is to say, the model can effectively predict the spot welding performance of the galvanized steel sheets. The forecasting precision is high enough to meet the practical need of engineering and has some application value.

Key words: body galvanized steel sheet; spot welding; artificial neural networks; prediction; optimization

Effects of uneven surface on ultrasonic testing results of defects close to surface GUO Li-wei, Gang Tie, Hu xin (State Key Laboratory of Advanced Welding Production Technology, Harbin Institute of Technology, Harbin 150001, China). p81—84

Abstract: Laser welding is an important method to join titanium alloy. The rigorous nondestructive test is necessary because pores are eaeily formed in the laser welding. The bad effects of uneven weld surface on the automatic ultrasonic inspection were summarized. The simulated practical sample was inspected through immersed ultrasonic testing technique at different point with different frequency probe. The defects images of weld were constructed using reasonable testing parameters and probe. The defect, which was located in 1.0-2.5 mm below the surface and whose diameter was bigger than 0.3 mm, can be detected, when the testing process was used to detect the T-shape Ti alloy laser welded joint. The experimental results show that a right frequency of probe can reduce the bad influence of uneven surface, which improves the reliability of ultrasonic test effectively.

Key words: immersed ultrasonic test; laserwelding; Ti alloy T joint; C-scan

Finite element analysis of pipe discontinuous and continuous butt welding ZHANG Guo-dong, ZHOU Chang-yu (College of Mechanical and Power Engineering, Nanjing University of Technology, Nanjing 210009, China). p85—88, 92

Abstract: Temperature and residual stress fields of industrial pipe discontinuous and continuous butt welding was simulated by ABAQUS. The physital properties of the material depead on the temperature, and the effects of environmental conditions on welding temperature filed, which were both considered in simulation. The heat amplitude curves loading method was applied to simulate the moving heat source. The multi-pass welding was simulated by the technique of element birth and death. A comparison of temperature and residual stress fields between discontinuous and continuous welding was carried out. Results indicated that the temperature was much lower while discontinuous welding, but lower axial residual stress can be gained by continuous welding. The annular stress of discontinuous and continuous welding did not have much affection for the pipeline. In addition, the temperature and residual stress field of starting welding point was analyzed. The inner wall residual stress was much higher in starting welding point.

Key words: discontinuous weld; continuous weld; temperature field; stress field; numerical simulation

Plasma beam welding of shape memory alloy XU Yue-lan[1], CHENG Zhi-fu[1], FAN Xiao-long[1], CHU Cheng-lin[2], WANG Shi-dong[2] (1. Department of Material Science and Technology, Nanjing University of Science and Technology, Nanjing 210094, China; 2. Material School, Southeast University, Nanjing 210006, China). p89—92

Abstract: With high-energy plasma beam method, the weldability of the TiNi shape memory alloy sheet was studied. The high-energy plasma beam equipment system was partly designed and founded. The relationship among parameters and its proper adjusting range are acquired. Thus the range of the parameters used in the engineering application was obtained. Some characteristics such as phase, microstructure, shape memory properties and tensile strength of the welded joint were discussed. Results show that the crystal grain in welded joint is large, and new phases such as Ni_3Ti and Ti_2Ni separate out. Furthermore, the welding heat-affected zone is narrow, and the welded joint shape restoration rate is 93.8% of the parent metal and the parent metal tensile strength is 1 205 MPa. After being kept at 500 ℃ for 1 hour, the tensile strength of welded joint reaches 750 MPa which is 62.2% of the parent metal and the fracture appears in the center of weld.

Key words: shape memory alloy; plasma beam; heat treatment

Analysis on welding cold crack sensibility of 10Ni8CrMoV steel DU Yi, ZHANG Tian-hong, ZHANG Jun-xu (Luoyang Ship Material Research Institute, Luoyang 471039, Henan, China). p93—96

Abstract: By using implant test, cold cracking sensibility of 10Ni8CrMoV high strength steel was analysed. At four welding conditions of non-preheating, preheating at 100 ℃, preheating at 150 ℃ and preheating at 150 ℃ then postheating 200 ℃× 2 h, the critical rupture stresses of implant test and the welding thermal cycling parameters were measured, and the fracture appearance were observed by scanning electron microscope. By all these, the welding cold crack sensibility of 10Ni8CrMoV steel was analysed comprehensively. The results showed that with the preheat temperature being increased, the critical ruptrue stresses of implant test are higher, and the areas of dimple are relatively increasing in fracture surfaces, and the rupture tendency is displayed from intergranular crack to transgranular crack to ductile rupture. 10Ni8CrMoV steel possesses a high cold cracking sensibility. Preheat and postheat treatment technologies can obviously improve the weldability of 10Ni8CrMoV steel.

Key words: 10Ni8CrMoV steel; implant test; cold crack sensibility; critical rupture stress

Fatigue properties improvement of welded structures by plasma spraying process WANG Bing-ying, HUO Li-xing, WANG